Taylor & Francis
Taylor & Francis Group

RESEARCH PAPER

OPEN ACCESS | Check for updates

Ribonuclease E strongly impacts bacterial adaptation to different growth conditions

Janek Börner [a]*, Tobias Friedrich [b,c]*, Marek Bartkuhn [b,d], and Gabriele Klug [a]

aInstitute of Microbiology and Molecular Biology, Justus-Liebig-University Giessen, Giessen, Germany; bBiomedical Informatics and Systems Medicine, Justus-Liebig-University Giessen, Giessen, Germany; cInstitute of Biochemistry, Justus-Liebig-University Giessen, Giessen, Germany; dInstitute for Lung Health, Giessen, Germany
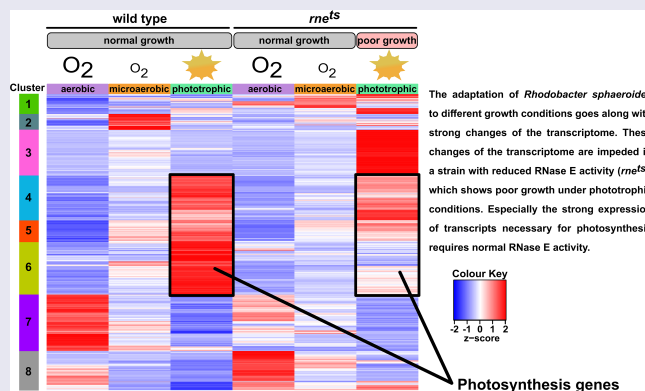
ABSTRACT

Adaptation of bacteria to changes in their environment is often accomplished by changes of the transcriptome. While we learned a lot on the impact of transcriptional regulation in bacterial adaptation over the last decades, much less is known on the role of ribonucleases. This study demonstrates an important function of the endoribonuclease RNase E in the adaptation to different growth conditions. It was shown previously that RNase E activity does not influence the doubling time of the facultative phototroph *Rhodobacter sphaeroides* during chemotrophic growth, however, it has a strong impact on phototrophic growth. To better understand the impact of RNase E on phototrophic growth, we now quantified gene expression by RNA-seq and mapped 5′ ends during chemotrophic growth under high oxygen or low oxygen levels and during phototrophic growth in the wild type and a mutant expressing a thermosensitive RNase E. Based on the RNase E-dependent expression pattern, the RNAs could be grouped into different classes. A strong effect of RNase E on levels of RNAs for photosynthesis genes was observed, in agreement with poor growth under photosynthetic conditions. RNase E cleavage sites and 5′ ends enriched in the *rne*ts mutant were differently distributed among the gene classes. Furthermore, RNase E affects the level of RNAs for important transcription factors thus indirectly affecting the expression of their regulons. As a consequence, RNase E has an important role in the adaptation of *R. sphaeroides* to different growth conditions.

The adaptation of *Rhodobacter sphaeroides* to different growth conditions goes along with strong changes of the transcriptome. These changes of the transcriptome are impeded in a strain with reduced RNase E activity (*rne*ts), which shows poor growth under phototrophic conditions. Especially the strong expression of transcripts necessary for photosynthesis requires normal RNase E activity.

Introduction

Rhodobacter sphaeroides (recently renamed *Cereibacter sphaeroides*; [1]) is a facultative photosynthetic bacterium that adapts its metabolism to the oxygen and light conditions in the environment. At high oxygen tension no photosynthetic complexes are synthesized and ATP is generated by aerobic respiration. When oxygen tension drops, photosynthetic complexes are synthesized, but also at low oxygen levels (microaerobic conditions) aerobic respiration can generate ATP. When no oxygen is present and light is available,

R. sphaeroides performs anoxygenic photosynthesis. In the absence of oxygen and light, fermentation or anaerobic respiration (in the presence of a suitable electron acceptor) can be performed. The photosynthetic complexes are assembled into an intracytoplasmic membrane system. At high or intermediate oxygen levels, formation of photosynthetic complexes is repressed by light [2,3]. This regulated formation of photosynthetic complexes by oxygen and light is important to avoid waste of energy for production of photosynthetic complexes when not required, but also to

avoid photo-oxidative stress by the simultaneous presence of light, oxygen, and bacteriochlorophyll.

The regulatory mechanisms allowing the adaptation of *R. sphaeroides* to different growth conditions and to photo-oxidative stress have been intensely studied in the past. Not only regulation at the level of transcription, e.g. by alternative sigma factors, is important during adaptation (e.g. [4–7]), but also post-transcriptional regulation. Especially during adaptation to stationary phase, we observed pronounced changes of the proteome that were not reflected by corresponding changes of the transcriptome [8]. Our studies revealed also the importance of riboregulation during adaptation of *R. sphaeroides* (e.g. [9–15]). Riboregulation includes regulation through the action of ribonucleases (RNases) and regulation by small non-coding RNAs (sRNAs).

Riboregulation in *R. sphaeroides* was already demonstrated decades ago: the distribution of RNA-stabilizing elements (secondary structures) and destabilizing elements (RNase cleavage sites) leads to *puf* mRNA segments with different stabilities (Figure S1; [16,17]; reviewed in [18]). The polycistronic *pufQBALMX* mRNA encodes proteins of the reaction centre (*pufLM*), of the light-harvesting I complex (*pufBA*), a scaffolding protein (*pufX*), and a protein regulating porphyrin flux (*pufQ*, [19]). More recently, in *R. sphaeroides* the sRNA PcrX was identified that is processed from the 3' UTR (untranslated region) of the *puf* operon by RNase E cleavage [12]. PcrX targets the *pufX* mRNA region, promotes its degradation and thereby also influences the amounts of photosynthetic complexes. Furthermore, the antisense RNA asPcrL affects RNase III-dependent decay of the *pufL* mRNA segment [13]. Differences in the stability of the *puf* mRNA segments contribute to the stoichiometry of reaction centre and light-harvesting complexes, and influence growth of *Rhodobacter* when shifted to phototrophic conditions [9]. It was also demonstrated that the rate of initial endonucleolytic cleavage by RNase E within the *pufBALMX* mRNA segment is influenced by the oxygen concentration in the environment [20].

Considering the impact of mRNA degradation on regulation of *puf* gene expression, the influence of RNase E on the transcriptome of *R. sphaeroides* was analysed on a global level by RNA-seq from cultures grown at microaerobic conditions [21]. Since the *rne* gene cannot be deleted, the native *rne* gene was replaced by the *rne-3071* gene from *E. coli* that leads to production of a temperature-sensitive RNase E. A transcriptome analysis was performed by RNA-seq under microaerobic conditions. Despite the higher GC content of its genome, *R. sphaeroides* RNase E, like the *E. coli* enzyme, targets AU-rich sequences [21]. A strong effect of altered RNase E activity on the transcriptome was observed at 42°C, but many changes also occurred at 32°C, the optimal growth temperature for *R. sphaeroides*. *E. coli* RNase E can be part of a degradosome, a multienzyme complex composed of RNases, helicases and metabolic enzymes (reviewed in [22]). Degradosome complexes with varying composition were also found in several alphaproteobacteria, including *Rhodobacter capsulatus* [23], but also in cyanobacteria and Gram-positives [22]. The *E. coli* (gammaproteobacterium) degradosome localizes to the cytoplasmic membrane, the degradosome of the alphaproteobacterium *Caulobacter crescentus* localizes to BR-bodies, ribonucleoprotein condensates in the interior of the cell [22].

The localization of the degradosome of the alphaproteobacterium *R. sphaeroides* has not been analysed. Under microaerobic and phototrophic conditions, the cells are filled with intracytoplasmic membranes that accommodate the photosynthetic complexes [24]. In contrast to the *E. coli* RNase E, the RNase E enzymes of the alphaproteobacteria have an arginine-proline-rich region inserted into the S1 domain [25].

The $rne^{E.\ coli\ (ts)}$ mutant of *R. sphaeroides* showed a pronounced phenotype regarding the formation of photosynthetic complexes and phototrophic growth, whereas there was no effect on chemotrophic growth under microaerobic conditions [21].

To better understand the strong effect of RNase E on phototrophic growth of *R. sphaeroides*, we compared RNA-seq data from the wild type and the rne^{ts} mutant not only during microaerobic (25–30 mM oxygen) growth at 32°C, but also under aerobic (160–180 mM oxygen), and phototrophic (no oxygen, 60 W/m^2 white light) growth conditions. We mapped 5' ends that are reduced in the mutant (log$_2$ fold change >1), indicating *bona fide* RNase E cleavage sites (scheme shown in Figure 1A). We also mapped 5' ends that are enriched in the rne^{ts} mutant. RNase E can bind to monophosphorylated 5' ends and will subsequently introduce cleavages in an overall 5'-3' direction (5' end-dependent degradation). Such monophosphorylated 5' ends can stem from previous endonucleolytic cleavage (by RNase E or RNase III) or by action of pyrophosphohydrolase on the 5' triphosphate of primary transcripts. Monophosphorylated 5' ends will be stabilized in the rne^{ts} mutant and are consequently enriched (Figure 1B).

Our data identified classes of genes with distinct RNase E-dependent expression patterns under different growth conditions. A strong impact of RNase E on expression of photosynthesis genes is in agreement with impeded growth under photosynthetic growth conditions. The effects of RNase E on mRNA classes (required for photosynthesis or motility) coincide with an effect of RNase E on the mRNAs for important transcriptional regulators for these classes.

Material and methods

Cultivation of bacterial strains

The *R. sphaeroides* 2.4.1 wild type ([26]; now renamed *Cereibacter sphaeroides*, [1]) and the *R. sphaeroides* rne^{ts} mutant [27] were cultivated in malate minimal medium [28] at 32°C. Both strains were either grown in the presence of high oxygen concentration of 180 µM dissolved oxygen (aerobic cultures), low oxygen concentration of 25 µM dissolved oxygen (microaerobic cultures) or in the absence of oxygen but illuminated with 60 W*m^{-2} white light (phototrophic cultures).

RNA isolation and RNA sequencing

20 ml of each culture were collected during exponential growth phase on ice at an OD$_{660}$ of 0.4. Afterwards, cells were sedimented by centrifugation at 10,000 rpm for 10 min at 4°C (Sorvall RC 6 Plus centrifuge, Thermo Scientific). For

total RNA isolation the hot phenol method [29,30] was used. For removal of remaining DNA from RNA isolates the Turbo DNA-*free* kit (Invitrogen) was used following the manufacturer's protocol. To test for remaining DNA, PCR with specific primers against *rpoZ* was performed. DNA-free RNA was tested for RNA integrity by electrophoresis of 1.5 μg sample on denaturing 10% polyacrylamide TBE gels and subsequent staining with ethidium bromide, as well as on the Bioanalyzer (described in the data generation description of our deposited RNA-seq data in the GEO repository). The sequencing libraries were constructed as described earlier [31], using the NEBNext Multiplex Small RNA Library Prep Set for Illumina (NEB).

Spike-in quantitative reverse transcriptase PCR (qRT-PCR)

For quantification of RNA abundances by qRT-PCR a spike-in approach was used. For this, 1 ng of DNA-free spike-in *in vitro* transcribed *sinI* RNA from *Sinorhizobium meliloti* was added to the harvested cell pellet prior to RNA isolation [14]. The subsequent qRT-PCR of DNA-free RNA isolates was performed using the Brilliant III Ultra-Fast SYBR Green QRT-PCR Master Mix kit (Agilent Technologies) following the manufacturer's protocol. Relative RNA abundances were calculated from independent biological triplicates, each in technical replicates, using the Pfaffl quantification model (with efficiency correction) [32].

RNA half-life determination

To monitor RNA decay over time, 20 ml samples of biological triplicates of wild type and *rne^ts* mutant were sedimented as described above. One sample of each culture, referring as t0 (100%), was collected immediately before addition of 0.2 mg/ml rifampicin (SERVA electrophoresis GmbH), while the following samples were collected at the time points 3 min (t1), 6 min (t2), 9 min (t3), 15 min (t4) and 30 min (t5) after addition of rifampicin. RNA isolation by hot phenol extraction and quantification by qRT-PCR were performed as described above.

RNA-seq data processing

Alignment of the raw sequencing reads against the reference genome of *R. sphaeroides* (NC_007493.2, NC_007494.2, NC_009007.1, NC_007488.2, NC_007489.1, NC_007490.2, and NC_009008.1) was performed using the READemption pipeline [33] v.1.0.5. The aligned reads were stored as binary alignment maps (BAM) files in the 'output/align/alignments' folder created by READemption. Those BAM files were further processed within R v.4.1.2 [34] using a systemPipeR [35] v.1.26.3 with custom made parameter files for the different tools. For the analysis of gene expression, the read counts per gene were calculated using the summarizedOverlaps function with the corresponding gene transfer file (GTF) for each BAM file. DESeq2 [36] v.1.32 was used for the normalization of the reads and the identification of transcriptional changes. DESeq2's $\log_2$ fold change and adjusted p-value (Benjamini and Hochberg) were used for the identification of significantly differentially expressed genes (results of the DESeq2 analysis are listed in supplement table S3). The prediction of TSS and 5'/3' UTRs was performed earlier [37].

In order to define *bona fide* cleavage sites or 5' ends enriched in the mutant, the strand-specific coverage of each base of the genome based on the 5' counts of each read was generated using bedtools [38] genomecov function with '-d −5 -ibam -strand' parameters and the corresponding genome. To exclude bases with an insufficient coverage, a single base must have at least 10 counts in one of the replicates of the different conditions to be used for the identification of *bona fide* cleavage sites or 5' ends enriched in the mutant. The coverage of the remaining bases was normalized and the changes for
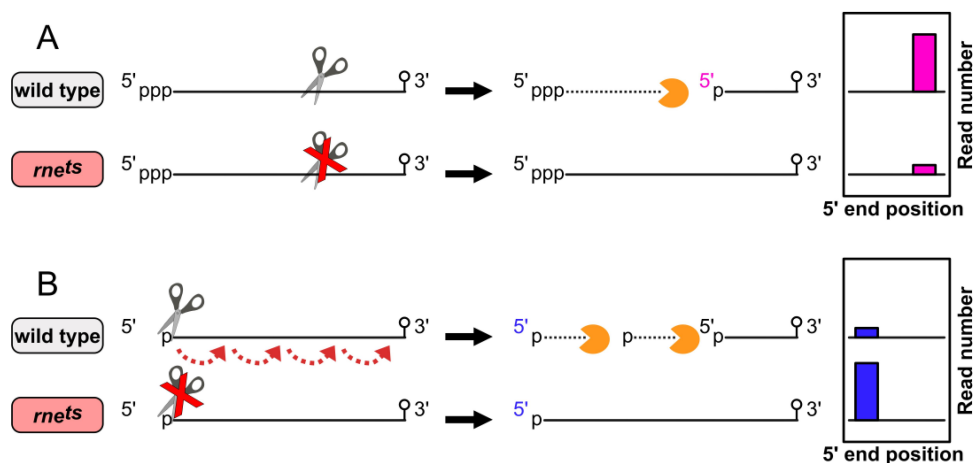

Figure 1. **Mapping of stable 5′ ends from RNA-seq data**. Schematic overview for the identification rules used for mapping of *bona fide* cleavage sites, and 5′ ends enriched in the *rne^ts* (modified from [21]). (A) Bacterial primary transcripts typically harbour triphosphorylated 5′ ends, and 3′ ends which are protected by RNA secondary structures like stem loops. Internal cleavage by RNase E generates monophosphorylated 5′ ends and unprotected 3′ ends. Subsequently, unprotected 3′ ends are rapidly degraded by 3′ to 5′ exoribonucleases like PNPase or RNase R. Due to reduced RNase E activity in the *rne^ts* mutant, less internal cleavage by RNase E is catalysed, consequently leading to lower amounts of newly generated stable 5′ ends in the *rne^ts* mutant (cleavage sites). (B) Since RNase E can be allosterically activated by monophosphorylated RNA substrates (5′ end-dependent pathway), which are generated by endoribonuclease or pyrophosphohydrolase activity, these transcripts tend to accumulate in the mutant and can be identified by enriched 5′ ends in the mutant.

each base between the rne^{ts} mutant and the wild type was calculated using DESeq2. Bases with a $\log_2$ fold change >1 and adjusted p-value <0.05 were defined as *bona fide* cleavage sites. 5' ends enriched in the mutant were defined using the same threshold for adjusted p-value but a $\log_2$ fold change < −1. Multiple adjacent cleavage sites or 5' ends enriched in the mutant within three bases to each other were reduced to one site using bedtools merge function with '-s -d 3 -o distinct' parameters.

The test for over representation of genes associated with GO terms (based on QuickGO taxon ID: 272943) for different groups of genes (e.g. significantly up-/downregulated) was performed using the fisher exact test for each GO term (pathway).

The GSEA was performed using the fGSEA R package [39] with gene sets based on all genes associated with a cleavage site or enriched 5' ends and the ranked list for all genes based on Wald statistic calculated by DESeq2.

p-values were normalized for multiple testing using the Benjamini and Hochberg strategy [40].

To compare the *rne* mRNA levels of the *E. coli* variant and the *R. sphaeroides* variant, the *E. coli* K12DH10B genome was downloaded from Illumina iGenomes. The sequence of the *E. coli* gene plus 500 bp upstream and downstream was extracted and added as a new chromosome to the FATSA file of *R. sphaeroides*. This combined FASTA file was used for alignment as described above. Counting of raw data for *E. coli* rne^{ts} mRNA reads and *R. sphaeroides rne* mRNA reads was performed using featureCounts from the Rsubread package [41]. These reads were size normalized and normalized for the longer length of the *E. coli* rne^{ts} gene.

RNase E activity reporter assay

For construction of the RNase E activity reporter, the mVenus open reading frame was cloned under transcriptional control of the strong constitutive 16S rRNA promoter (control plasmid). To monitor RNase E activity the well characterized RNase E cleavage site of the small RNA UpsM from *R. sphaeroides* [14] was introduced into the 5' UTR. All primers used for the cloning of the reporter plasmids are listed in supplement table S4. A scheme of the used constructs is depicted in Figure S2.

The sequence of the 16S rRNA promoter was amplified from the *R. sphaeroides* 2.4.1 genome by PCR using the oligonucleotides p16S_HindIII_for and p16S_ScaI_rev. The amplicon was inserted into pPHUmVenus [42] with *Hind*III and *Sca*I resulting in the plasmid pPHU231-p16S-mVenus (control plasmid). Subsequently, an 89 bp DNA fragment of the UpsM sequence was amplified using the primers UpsM90_ScaI_for and UpsM90_XbaI_rev, followed by insertion into pPHU-p16S-mVenus via *Sca*I and *Xba*I yielding the plasmid pPHU231-p16S-UpsM90-mVenus.

The plasmids pPHU231-p16S-mVenus and pPHU231-p16S-UpsM-90-mVenus were separately transferred into *R. sphaeroides* wild type and the rne^{ts} mutant by diparental conjugation using *E. coli* strain S17–1 [43]. Biological triplicates of the conjugants were cultivated under aerobic, microaerobic or phototrophic conditions. 100 μl of exponentially grown cultures were transferred into 96-well plates as technical duplicates, followed by measurements of OD_{660} and fluorescence of mVenus (extinction 515 nm, emission 548 nm) in a Tecan Infinity plate reader. The samples of phototrophic cultures were incubated at room temperature for 10 min after transfer into 96-well plates prior to the measurements, allowing maturation of mVenus fluorophore by oxygenation. As a control of background autofluorescence signals, empty vector controls of wild type and rne^{ts} mutant were cultivated and analysed according to the same described procedure.

Results and discussion

Effect of different growth conditions on the transcriptome of R. sphaeroides

We observed previously that reduced RNase E activity has a large impact on growth of *R. sphaeroides* under phototrophic, but not under chemotrophic growth at low oxygen tension (microaerobic conditions). In the previous study, the effect of RNase E on the transcriptome was only investigated under chemotrophic (microaerobic) conditions [21]. To better analyse the impact of RNase E on adaption of *R. sphaeroides* to different growth conditions, we now compared RNA-seq data of wild type and rne^{ts} mutant under phototrophic conditions and microaerobic conditions and also included chemotrophic growth under high oxygen tension (aerobic growth). Figure 2 demonstrates that growth behaviour under aerobic or microaerobic conditions is very similar in *R. sphaeroides* wild type, and growth of the rne^{ts} mutant is comparable. Under the chosen light condition, the wild type reaches a higher optical density when grown phototrophically. As already reported previously [21], the rne^{ts} mutant is strongly impeded in growth under these conditions.

To understand, why lower RNases E activity especially affects phototrophic growth, for each growth condition three RNA samples were analysed by RNA-seq, originating from three independent biological replicates. The PCA plot shown in Figure 3A demonstrates the good reproducibility of the sequencing triplicates. As expected, the highest variance between the different samples is based on the different growth conditions (aerobic, microaerobic, phototrophic) of *R. sphaeroides*. Of note, the microaerobic samples are in between the aerobic and phototrophic conditions, highlighting this intermediated growth condition. Interestingly, clear differences between rne^{ts} mutant and wild type samples are detectable for all conditions, suggesting that the enzyme mediates mild, albeit consistent effects under chemotrophic conditions, too. In line with the growth curve (Figure 2), the effects of the rne^{ts} mutant are by far the most visible under phototrophic growth conditions.

The influence of growth conditions on the transcriptome of *R. sphaeroides* wild type is also shown in Figure 3B. There is little change of the transcriptome when aerobic and microaerobic conditions are compared: about 90% of the genes show similar expression levels ($\log_2$ fold change >−1 and <1). 5% of the genes show significantly lower expression under aerobic conditions ($\log_2$ fold change <−1 and adjusted p-value <0.05), 4.6% of the genes show significantly higher
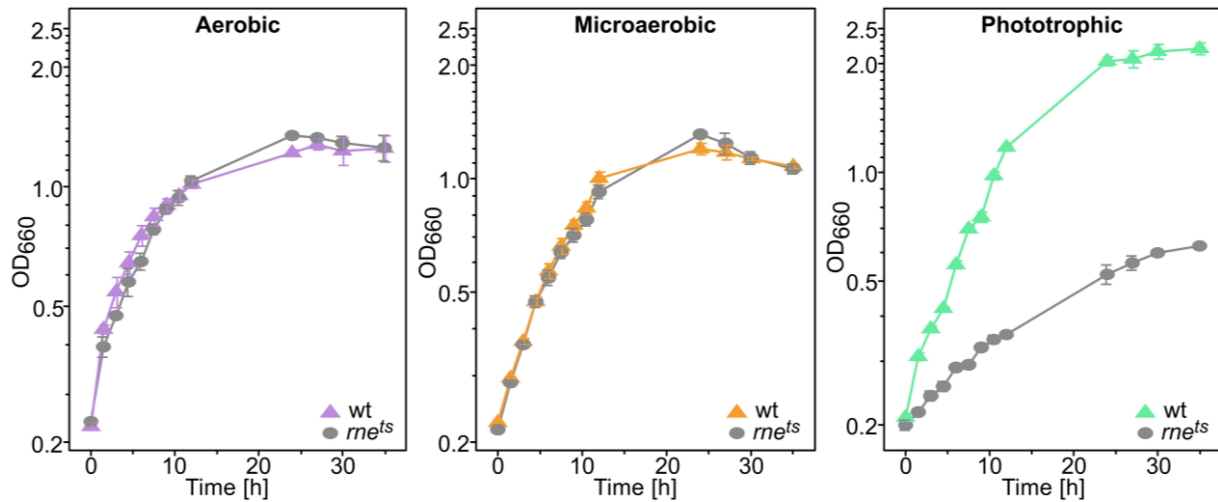
Figure 2. Growth behaviour of *R. sphaeroides* wild type and *rne^ts* mutant under aerobic, microaerobic, and phototrophic growth conditions. Exponentially grown pre-cultures were diluted to an OD_{660} of 0.2 and growth was followed by measuring the optical density (OD_{660}) of *R. sphaeroides* wild type and *rne^ts* mutant cultures for 35 hours. The mean and standard deviation of independent biological triplicates is shown.
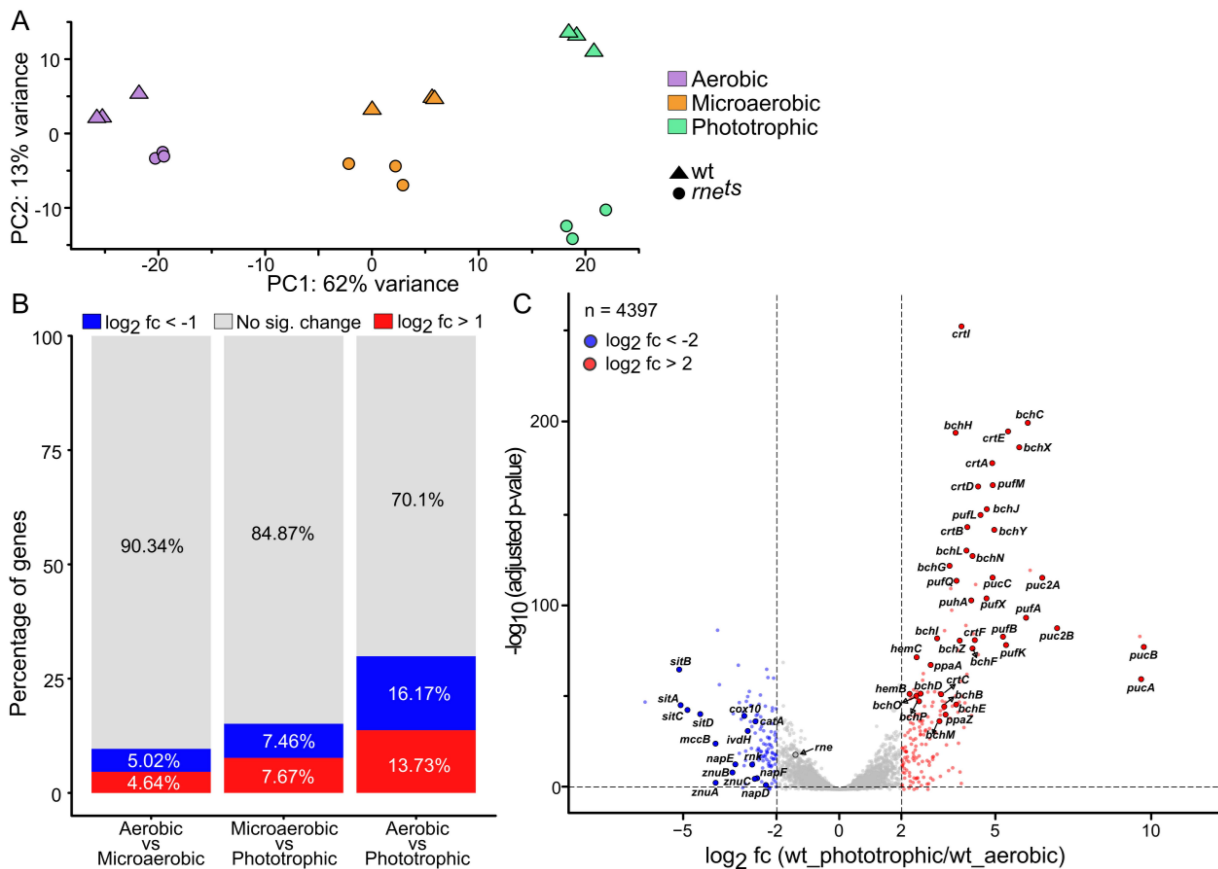

Figure 3. Significantly differentially expressed genes in *R. sphaeroides* among different environmental conditions. (A) Principle component analysis (PCA) showing the variation of the transcriptome of the two *R. sphaeroides* strains (wild type and *rne^ts* mutant) under aerobic, microaerobic, and phototrophic growth conditions. The transcriptome was analysed by RNA-seq. (B) Percentage of significantly differentially expressed genes in comparison between aerobic, microaerobic, and phototrophic growth conditions of *R. sphaeroides* wild type, including all genes with adjusted p-value <0.05 and log_2 fold change >1 (upregulated) or <−1 (downregulated). (C) Volcano plot highlighting significantly differentially expressed genes between phototrophic and aerobic growth conditions.

expression (log_2 fold change >1 and adjusted p-value <0.05). When microaerobic and phototrophic growth conditions are compared, differences in the transcriptome are slightly larger. About 7.5% of all genes show significantly lower expression

under microaerobic conditions and about 7.7% of the genes show significantly higher expression. Expression levels show much stronger differences between aerobic and phototrophic conditions: 16.2% of the genes show significantly lower

expression levels under aerobic conditions, 13.7% show significantly higher expression levels.

This result reflects, that the change of parameters concerning oxygen concentration and light between aerobic and phototrophic growth is the biggest. In previous work, *R. sphaeroides* transcriptomes under different growth conditions were analysed using microarrays. Pappas et al. (2004) reported decreased expression of about 10% of the transcripts in aerobic cultures versus phototrophic cultures, and increased expression levels for about 12% of the transcripts. These changes are in the same range as observed in our data set.

The different expression pattern between phototrophic and aerobic conditions is further visualized in a volcano plot (Figure 3C). Among the genes with significantly higher expression (log$_2$ fold change >2 and adjusted p-value <0.05) under phototrophic conditions are many photosynthesis genes (45 genes of a total of 180): *puf* and *puc* genes encoding pigment-binding proteins, *bch* genes for bacteriochlorophyll synthesis, *hem* genes for the synthesis of protoporphyrin IX, *crt* genes for carotenoid synthesis, *ppaA* for a transcriptional regulator of photosynthesis genes. The products of those genes are required for phototrophic growth but not or to a lesser extent under aerobic conditions, when the presence of photosynthetic complexes may cause photo-oxidative stress. Similar expression patterns were also observed in a previous microarray study [44]. Strongly reduced expression levels under phototrophic growth are observed e.g. for a number of genes for ribosomal proteins or genes involved in metal transport (*sit, zur, exbD*). Interestingly the *rne* transcript shows higher abundance (2.7-fold) under aerobic conditions than under phototrophic conditions.

Figure S3 shows the result of a gene ontology term enrichment analysis including all significantly upregulated genes as shown in the volcano plot (Figure 3C). This analysis also confirms a significant role of those RNAs in photosynthesis and closely associated functions.

Effect of RNase E on global changes of the transcriptome under different growth conditions

As a next step we compared the changes of the transcriptome under different growth conditions in the wild type and the *rne*^{ts} mutant strain (Figure 4A). Only transcripts with a strong and statistically significant differential expression (log$_2$ fold change >2 or <−2 and adjusted p-value <0.05) between growth conditions or strains are included (446 transcripts in total). The left part of the figure shows the expression profiles in the wild type. Individual expression levels are compared to the average (colour coded). Based on their expression pattern under different growth conditions and in different strains the transcripts are grouped into eight different clusters by unsupervised agglomerative hierarchical clustering. When microaerobic and aerobic conditions are compared in the wild type, major changes occur in cluster 2, which shows much stronger expression under microaerobic conditions, and in cluster 7, which shows much stronger expression under aerobic conditions. When microaerobic and phototrophic conditions are compared, the change in expression pattern is more drastic: clusters 4, 5, and 6 show strongly increased expression under phototrophic conditions, transcript levels of clusters 7 and 8 are rather decreased.

Our previous study focused exclusively on the identification of differential 5' ends, which are affected by RNase E in
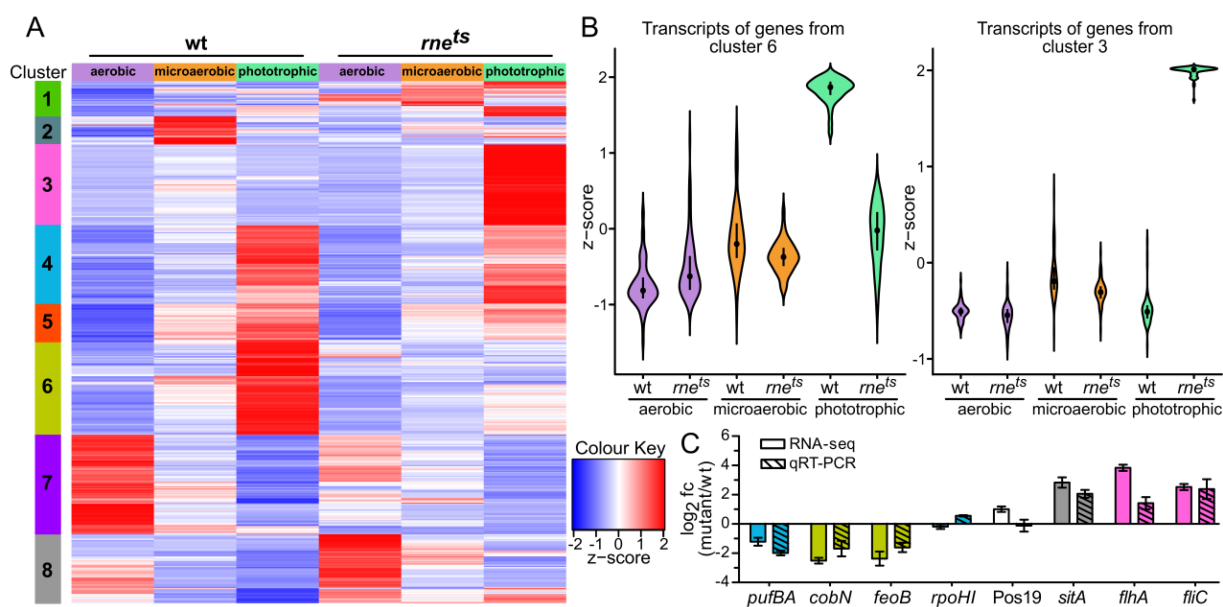

Figure 4. The *rne*^{ts} mutant has a highly altered transcriptome, especially under phototrophic conditions. (A) Heatmap illustrating the z-standardized transcriptomic changes of transcripts of the top deregulated genes (adjusted p-value <0.05 and log$_2$ fold change >2 or <−2; n = 446) based on all growth conditions, highlighting transcriptomic changes among aerobic, microaerobic, and phototrophic growth conditions of *R. sphaeroides* wild type and the *rne*^{ts} mutant. The clustering was performed according to the Euclidean distance. (B) Quantification of the z-standardized gene expression of RNAs from cluster 6 and cluster 3 (as shown in panel A). (C) Spike-in quantitative reverse transcriptase PCR with total RNA obtained from phototrophically grown wild type and *rne*^{ts} mutant. The relative abundance of selected RNAs (bars are coloured according to the clusters of the heatmap) in the *rne*^{ts} mutant, is shown.

R. sphaeroides under microaerobic conditions [21]. In this study, we were also interested in differential 5' ends under aerobic and phototrophic conditions, and especially in RNA expression levels in the mutant under the different growth conditions. The right part of Figure 4A shows the expression levels under the three growth conditions for the *rne*[ts] mutant. The expression profiles shown in Figure 4A clearly demonstrate a particularly strong impact of RNase E under phototrophic conditions. In microaerobic conditions, the expression profiles are quite similar between the two strains. Major differences occur in cluster 2 which shows clearly lower expression when RNase E activity is reduced and in cluster 1 with higher expression in the mutant. Cluster 2 comprises 24 genes, of which 12 encode hypothetical proteins (Table S1). Two genes encode Fru-1,6-bisphospatase, two encode uncharacterized transcriptional regulators, two encode subunits of ABC transporters, one encodes a protein for conjugational transfer. Further annotations are: putative chemoreceptor protein, metalloprotease, NADH-ubiquinone oxidoreductase subunit, fosmidomycin resistance protein, D-malate dehydrogenase.

Cluster 1 comprises 29 genes, four of them for tRNAs (Table S1). 14 genes encode hypothetical proteins, two genes flagellar proteins and nine genes proteins of various predicted functions. RSs_1624 is a UTR-derived sRNA. Due to the lacking characterization of most proteins, the biological consequences of changed transcript levels of cluster 1 and 2 remain elusive.

Under aerobic conditions cluster 7 shows very strong expression in the wild type, which is much weaker in the *rne*[ts] mutant. 85 genes belong to this cluster, among them the *rne* gene for RNase E, the *rnpA* gene for the RNase P protein component, RSP_0624 coding for RNase G, nine genes for ribosomal proteins, two for sRNAs, and 29 genes encoding hypothetical proteins. Considering the *rne* gene, the RNA-seq results cannot be compared between wild type and mutant, since the *rne*[ts] transcript of the mutant only partly maps to the *R. sphaeroides* genome. Other genes in cluster 7 encode proteins with unknown or diverse metabolic or regulatory functions (Table S1). Cluster 8 comprises 59 genes and shows clearly stronger expression under aerobic conditions than in other growth conditions in the mutant, but only slightly increased expression in the wild type. Like in cluster 7, many mRNAs of cluster 8 encode proteins with unknown (23 hypothetical proteins) or diverse metabolic or regulatory functions (Table S1). Furthermore, cluster 8 includes genes encoding catalase (*catA*), nitrate reductase (*napBDEF*), pyrroloquinoline quinone biosynthesis proteins (*pqqACD*), several proteins involved in metal transport (*sitACD, znuABC, zur*), sugar transport (RSP_2367, 2368), subunits of a TRAP-T transporter (RSP_1418–1420), and two predicted transcriptional regulators (RSP_2950 and RSP_3448).

Under phototrophic conditions cluster 4, 5, and 6 are strongly induced in the wild type. There is weaker induction of cluster 4 and 5 genes in the mutant, but no or only very weak induction of cluster 6 under phototrophic conditions. Cluster 6 comprises 81 genes, about 20 encode proteins with known functions in photosynthesis. They are required for syntheses of bacteriochlorophyll, carotenoids, protoporphyrin and cobalamin (which is required for bacteriochlorophyll

synthesis, reviewed in [45]), or the synthesis of pigment-binding proteins. 17 genes with a role in photosynthesis are also found in cluster 4, which comprises 67 genes including six genes for sRNAs of unknown function. Cluster 4 includes most *puf* and *puc* transcripts that encode pigment binding proteins, *bchD* and *bchI* for bacteriochlorophyll synthesis, *hemC* encoding porphobilinogen deaminase, and *cycA* and *cycC* encoding cytochrome c_2 that is required for photosynthetic electron transport. Interestingly, the transcript encoding the alternative sigma factor RpoHI is also part of cluster 6. RpoHI has an important function in many stress responses, including photooxidative stress and stationary phase [6,31,37,46,47]. The association of cluster 6 and cluster 3 genes with different GO terms is shown in Figure S4.

Expression of cluster 6 and cluster 3 genes is also visualized in the violin plot in Figure 4B. It underlines the similar expression of the clusters in mutant and wild type in aerobic and microaerobic conditions but very different expression patterns during phototrophic growth.

Cluster 5 comprises only 31 genes, half of them with a role in pigment synthesis, three genes for proteins required for formation of photosynthetic complexes (*pucC, pufQ*, RSP_0276).

Considering the high number of genes required for photosynthesis in clusters 4–6, the poor growth of the *rne*[ts] mutant under phototrophic conditions is not surprising.

Very pronounced differences in expression between mutant and wild type under phototrophic conditions are also seen for cluster 3, which consists of 69 genes and shows much stronger expression in the mutant. 12 genes encode hypothetical proteins, 48 genes encode proteins for flagellar synthesis or chemotaxis. Expression of cluster 3 genes is rather similar in the wild type under all three conditions and also between wild type and mutant during chemotrophic growth. This is also visualized by the violin plot in Figure 4B.

For some selected genes we confirmed the expression changes between mutant and wild type for phototrophic growth by real-time RT-PCR (Figure 4C). The DESeq2 analysis quantifies all reads obtained for a gene, while in the real-time RT-PCR expression of only a small part of an RNA (about 200 nt) is monitored. This may account for slight differences in the observed expression changes between the two methods.

Cleavage by RNase E is strongly influenced by growth conditions

As a next step, *bona fide* RNase E cleavage sites (5' ends significantly reduced in *rne*[ts] mutant: $\log_2$ fold change <-1 and adjusted p-value <0.05) were identified for the different data sets, as well as the 5' ends that are significantly enriched in the mutant ($\log_2$ fold change >1 and adjusted p-value <0.05) (Figure 5). By far the most cleavage sites were detected under aerobic conditions (4206 total), followed by phototrophic conditions (2765 total) and microaerobic conditions (2007 total) (Figure 5A). For an important and validated cleavage site of RNase E within *pufL* in *R. capsulatus* an influence of oxygen tension during growth on cleavage was already noted decades ago [20]. This study demonstrates for
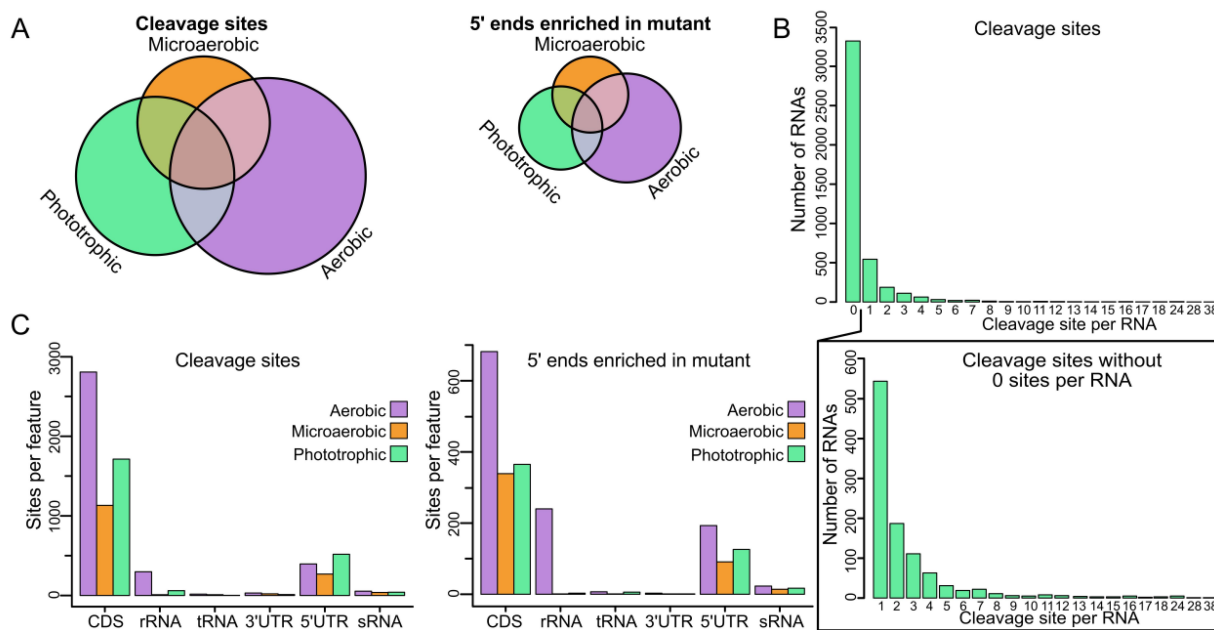
Figure 5. **RNA-seq based identification of** *bona fide* **RNase E cleavage sites and enriched 5' ends in the mutant.** (A) Number of mapped RNase E cleavage sites and enriched 5' ends in the mutant under aerobic, microaerobic, and phototrophic growth conditions. The circles and their overlaps are proportional according to the amount of identified sites. (B) Number of RNAs with mapped cleavage sites under phototrophic conditions. A magnified version is depicted in the lower panel, missing RNAs without cleavage sites. (C) Distribution of cleavage sites and enriched 5' ends in the mutant among annotated genomic features.

the first time a major influence of growth conditions on RNase-mediated processing and maturation.

With 1108 mapped cleavage sites, the overlap between aerobic/microaerobic conditions was the biggest, whereas for microaerobic/phototrophic conditions an overlap of 905 cleavage sites, and for aerobic/phototrophic conditions an overlap of 569 cleavage sites was identified. In total, less 5' ends enriched in the mutant were detected than cleavage sites, while the distribution among the different growth conditions was similar.

No RNase E cleavage sites were mapped for a high percentage of transcripts (about 2700 under all conditions; about 3300 under phototrophic conditions). This implies that many changes in the transcriptome are rather due to altered production of the transcripts or to turn-over by other RNases than to altered turn-over by RNase E. However, not all existing cleavage sites will meet our criteria ($\log_2$ fold changes and p-values). Nevertheless, they may contribute to turn-over of transcripts. Unexpectedly, the overlap of cleavage sites in different growth conditions was also rather small: 2830 cleavage sites were detected only in aerobic conditions, 1535 cleavage sites only in phototrophic conditions, which could be due to generally differential RNA abundances between the three conditions, a fact that may influence the likelihood to map *bona fide* cleavage sites. Since the mutant showed a strongly impaired growth phenotype under phototrophic conditions, we were especially interested in the distribution of cleavage sites per RNA during phototrophic growth (Figure 5B). While most RNAs (about 3300) were found to harbour no *bona fide* cleavage site (by our definition), we observed a wide spread distribution of cleavage sites per RNA for those RNAs with cleavage site(s). For a majority of

RNAs 1–7 cleavage sites were mapped, while we also found RNAs with over 20 *bona fide* cleavage sites per RNA.

In addition to the number of cleavage sites per RNA under phototrophic conditions, we investigated the distribution of all cleavage sites and 5' ends significantly enriched in the mutant under aerobic, microaerobic and phototrophic conditions among annotated genomic features (Figure 5C). For all three conditions, most cleavage sites were mapped within coding sequences (CDS), followed by 5' UTRs and rRNAs, except for aerobic conditions where we mapped an unexpected high number of enriched 5' ends in the mutant within rRNAs. In comparison with our previously published data [21], the distribution of sites among genomic features is generally similar. rRNAs are part of large transcripts that undergo several maturation steps including the action of RNase E, RNase III, RNase P and RNase J [48–51]. These processes generate many intermediate and mature monophosphorylated 5' ends, which are likely to accumulate in the *rne*[ts] mutant. Although previous microarray data indicated that rRNA/total RNA ratios did not change drastically between different growth conditions [52], the enrichment of these rRNA 5' ends under aerobic conditions in the mutant remains to be elucidated. Nevertheless, a biological effect on the growth behaviour caused by the higher amounts of rRNA 5' ends mapped under aerobic conditions in the mutant was not visible (Figure 2).

We also analysed the correlation of cleavage site distribution and differences in gene expression between the *rne*[ts] mutant and the wild type under phototrophic growth conditions. Most RNAs with mapped RNase E cleavage sites do not show significantly increased or decreased expression levels in the mutant under phototrophic
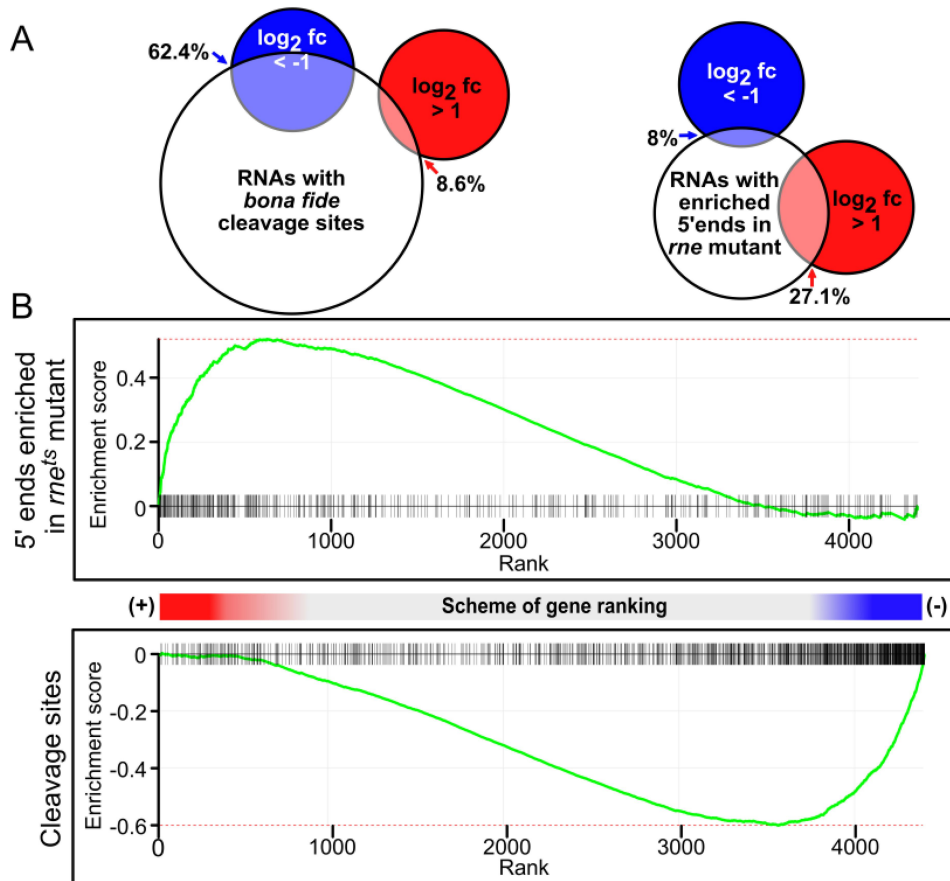
Figure 6. **RNAs with cleavage sites significantly correlate with weakly expressed genes in the mutant under phototrophic conditions**. (A) Overlap of significantly differentially expressed genes (mutant/wild type) with RNAs harbouring cleavage sites or enriched 5' ends in the mutant under phototrophic conditions, including all RNAs with adjusted p-value <0.05 and log$_2$ fold change >1 or <−1. (B) Gene set enrichment analysis (GSEA) including all genes of *R. sphaeroides*. The distribution of cleavage sites (bottom panel) or 5' ends enriched in the mutant (top panel) within the DESeq2 ranked gene list was analysed. The RNAs were ranked based on their expression changes according to the Wald statistics calculated by DESeq2 between both strains under phototrophic conditions. Each black line represents an RNA. RNAs with highest expression (*rne^{ts}*_phototrophic/wt_phototrophic) are localized at the red end of the gene ranking scheme, whereas RNAs with lowest expression are localized at the blue end. The enrichment score is a running sum, which increases if an RNA possesses a cleavage site or mutant enriched 5' end.

conditions. Interestingly, 62.4% of all RNAs with decreased levels in the mutant (adjusted p-value <0.05 and log$_2$ fold change <−1) under phototrophic conditions contain RNase E cleavage sites (Figure 6A), while only 8.6% of the RNAs with increased expression in the mutant (adjusted p-value <0.05 and log$_2$ fold change >1) under phototrophic conditions contain RNase E cleavage sites. A different result is seen for 5' ends that are enriched in the mutant: Only 8% of the RNAs with decreased levels in the mutant under phototrophic conditions contain enriched 5' ends in the mutant, while 27.1% of the RNAs with increased level contain enriched 5' ends. In addition, the median log$_2$ fold change of all genes with mapped cleavage sites is about −0.4 (*rne^{ts}*_phototrophic/wt_phototrophic), while genes with enriched 5' ends in the mutant show a slight increase with a median log$_2$ fold change of about 0.2 (Figure S5). Considering that we identified 1040 RNAs with cleavage sites and 436 RNAs with enriched 5' ends in the mutant under phototrophic conditions, these median log$_2$ fold changes of such a number of RNAs are remarkable.

In order to further analyse the distribution of cleavage sites and enriched 5' ends in the mutant on a global scale, we performed a gene set enrichment analysis (GSEA) (Figure 6B). Here, we ranked all RNAs based on their expression change between *rne^{ts}* mutant and wild type under phototrophic conditions from maximal increased ratio (red) to maximal decreased ratio (blue) (Scheme of gene ranking), according to the DESeq2 analysis (Wald statistic). Next, we defined sets of RNAs based on association with cleavage sites or enriched 5' ends in the mutant, respectively. The enrichment score is a running sum, which increases if an RNA possesses an enriched 5' end in the mutant (top panel) or cleavage site (bottom panel), and decreases if an RNA does not possess any of both sites. Transcripts with and without cleavage sites are equally distributed among RNAs with highly increased expression in the mutant under phototrophic conditions (rank 0 to ~600) reflected by the straight line. Among the RNAs with ranks in between rank ~600 to ~3500 transcripts without cleavage sites dominate, leading to a decrease of the enrichment score. Among the RNAs with highest rank (rank

~3500 to ~4300; strongest decreased expression mutant versus wild type) many transcripts have cleavage sites, leading to a strong increase of the enrichment score. In conclusion, we compared both sets of RNAs with the ranked list and found both sets globally associated, with induced expression for enriched 5' ends in the mutant (p-value $<10^{-10}$) or reduced expression for cleavage sites (p-value $<10^{-10}$). These results show, that RNAs with diminished abundances in the mutant possess a particularly high amount of cleavage sites, which was also indicated as highly significant by hypergeometric test (enrichment over background distribution of cleavage sites: 6.23-fold; p-value $<2.2^{-16}$). *Vice versa*, RNAs with elevated abundances in the mutant were found to have a high number of 5' ends enriched in the mutant.

We also compared the number of cleavage sites and enriched 5' ends in each cluster of the heatmap to the mean distribution for each growth condition (Figure S6; Table S2). About 50% of the cleavage sites (cluster mean) of the mean background distribution were detected for cluster 6 transcripts under aerobic conditions but 2.7-fold (266%) more cleavage sites under microaerobic conditions, and even 7-fold (708%) more cleavage sites under phototrophic conditions (Figure S6; Table S2). Compared to the background mean over all transcripts, less enriched 5' ends were detected in cluster 3 (cluster mean) under aerobic and microaerobic conditions but almost twice as much 5' ends were enriched in phototrophic conditions (Figure S6; Table S2).

One concern in our analysis was that in general more RNase E cleavage sites and more enriched 5' ends in the mutant may be detected when the RNA levels between mutant and wild type show stronger variation. Cleavage sites may be mapped when transcript levels are much higher in the wild type than in the mutant and *vice versa* for enriched 5' ends in the mutant. This is already partially excluded by the GSEA shown in Figure 6, as also many cleavage sites are found in transcripts with increased levels in the mutant. Additionally, Figure S6 shows that such a correlation between expression change and number of cleavage sites is visible in some but not all cases. E. g. quite often both, cleavage sites and enriched 5' ends are increased under the same condition. Cluster 1 shows higher expression under phototrophic conditions in the mutant, but no cleavage sites are detected under phototrophic conditions. Cluster 8 shows similar expression in both strains under microaerobic conditions, but the number of enriched 5' ends in the mutant is 5-fold above background level.

To further exclude that the change of read number between wild type and mutant leads to changed levels in the detected 5' ends, we plotted the number of cleavage sites per RNA against the $\log_2$ fold change of the RNA between wild type and *rne*[ts] mutant under phototrophic conditions. As seen in Figure S7 no correlation between the fold change of an RNA and the number of detected cleavage sites is visible. Taken these results together, we conclude that the accumulation or reduction of cleavage sites and enriched 5' ends in the mutant observed in the clusters is not an artefact of the analysis. Note that in contrast to the GSEA (Figure 6B), the analysis shown in Figure S7 does not include RNAs without cleavage sites.

Levels of mRNAs for regulators of photosynthesis and motility gene expression are affected by RNase E

The effect of RNase E on the level of a certain mRNA may be direct by the processing of this particular mRNA. Our results support some correlation between the presence of RNase E cleavage sites or enriched 5' ends and expression change between microaerobic and phototrophic growth conditions (Figure S5; Figure 6B). Another possibility is an indirect effect through RNase E-mediated cleavage of an mRNA for e.g. a transcriptional regulator of this RNA. The fact that some of the clusters defined in Figure 4A contain many mRNAs with similar function and/or transcribed from the same chromosomal locus, supports the presence of such indirect effects in addition to the direct effects. Therefore, we gave special attention to the effect of RNase E on mRNAs for known regulators of photosynthesis gene expression.

PrrB/PrrA (sensor kinase and response regulator of a two-component system), PpsR/AppA, and FnrL (transcriptional activator) are important protein regulators that affect expression of many photosynthesis genes (overview shown in Figure 7). Real-time RT-PCR quantification confirmed a reduction in the levels of *prrB* and *appA* mRNAs between *rne*[ts] mutant versus wild type under phototrophic conditions (Figure 8). While the RNA-seq read coverage (Figure S9) showed similar abundances for the *appA* transcript in wild type under microaerobic and phototrophic conditions, *appA* mRNA was clearly less abundant in the *rne*[ts] mutant under phototrophic conditions. The *prrB* transcript showed higher abundance under phototrophic conditions in the wild type but not or to a lesser extent in the mutant (Figure S8). Since PrrB as well as AppA are important regulators of photosynthesis gene expression, the effect of RNase E on their transcript levels will indirectly affect expression of many photosynthesis genes (Figure 7). As a result of PrrB/PrrA being activators and AppA an antirepressor, higher levels of these proteins in the wild type will lead to stronger activation of photosynthesis genes in comparison to the mutant.

Although our study focused on the impact of RNase E on phototrophic growth, our data also revealed a strong influence of RNase E on genes of cluster 3, which was opposite to the effect seen on photosynthesis genes (Figure 4A,B) and includes many motility genes. Figs. 8 and S10 show that *rpoN2* mRNA is much more abundant in the mutant than in the wild type under phototrophic conditions. The alternative sigma factor RpoN2 is the master regulator of flagellar and motility genes [53–55], which are part of cluster 3 and show much stronger expression in the mutant under phototrophic conditions (Figure 4A).

How does RNase E affect mRNA levels of regulators of photosynthesis or motility genes?

Transcriptional start sites have been previously mapped for the *R. sphaeroides* transcriptome [37]. For the *appA* mRNA RNase E cleavage sites were mostly detected in the 5' UTR, which is transcribed from a promoter with the −35 region located around position 156.784. The screen shot in Figure S9
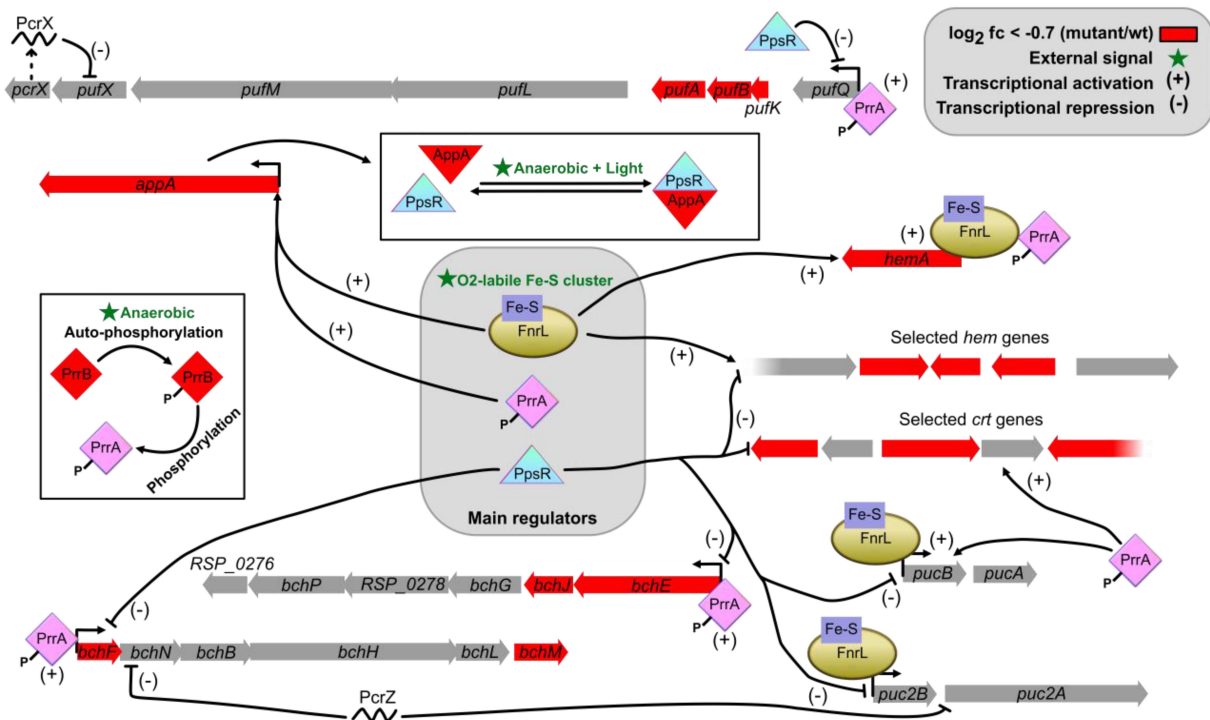
Figure 7. Schematic representation of the photosynthesis gene transcription regulation model in *R. sphaeroides*. The transcription of photosynthesis genes is controlled by multiple different activators and repressors to ensure a tight regulation upon changing environmental conditions. The regulation network consists of three main regulatory systems which are able to sense and signal changes in oxygen and light availability: (1) the activating PrrA/PrrB two component system senses oxygen availability, (2) the activator FnrL, which senses oxygen availability by an oxygen labile iron sulphur cluster, (3) the PpsR/AppA repressor/anti-repressor system which senses light and oxygen availability by a BLUF- and a SCHIC-domain, respectively, within the anti-repressor AppA. On post-transcriptional layer small regulatory RNAs (like PcrZ and PcrX) where found to fine-tune photosynthesis gene expression. RNAs with $\log_2$ fold change <-0.7 (rne^{ts}_phototrophic/wt_phototrophic) are marked in red colour.
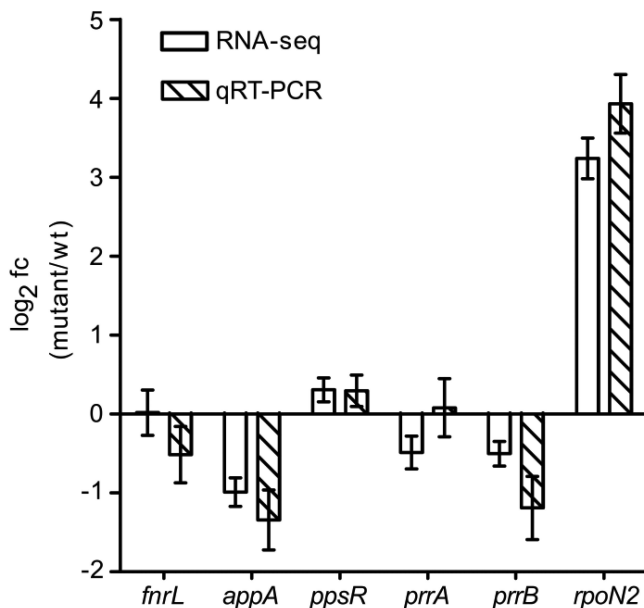

Figure 8. qRT-PCR for quantification ofmRNAs encoding transcriptional main regulators. Spike-in quantitative reverse transcriptase PCR with total RNA obtained from phototrophically grown wild type and rne^{ts} mutant. The relative abundances (mutant/wt) were calculated from independent biological triplicates.

shows that the distribution of RNase E cleavage sites differs between microaerobic and phototrophic conditions. Cleavage sites at positions 156.448, 156.587 and 156.478 were only mapped under phototrophic conditions. However, we cannot directly link cleavage site distribution to mRNA levels. Other cleavage sites were only mapped under microaerobic conditions. *prrB* is also transcribed from an own promoter with the −35 region around position 105.845 (Figure S8). The first two nucleotides of the *prrB* mRNA were mapped as RNase E cleavage sites, although the first nucleotide (transcription start site: TSS) is rather expected to be enriched in the rne^{ts} mutant, due to the impeded 5' end-dependent decay. In addition, RNase E cleavage sites are mapped to two further positions within the 5' UTR. Another RNase E cleavage site occurs only under phototrophic conditions at position 106.116 (Figure S8).

An influence of RNase E on the level of gene expression is likely to be due to an effect on transcript stability. To test this, we determined the half-lives of *appA* and *prrB*, in wild type and mutant under microaerobic and phototrophic growth (Figure 9). The half-life of *appA* under phototrophic conditions in the wild type was longer (about 4 min) than that in the rne^{ts} mutant (about 2 min 15 sec). The half-life of *prrB* was also clearly shorter under phototrophic conditions in the rne^{ts} mutant (1 min 35 sec) than in the wild type (about 3 min). Thus, both transcripts showed faster turn-over in the mutant under phototrophic conditions.

In agreement with the different expression patterns of cluster 6 and cluster 3 RNAs, the expression pattern of *rpoN2* mRNA is different from that of *appA* and *ppsR*: under phototrophic conditions *rpoN2* levels are much higher
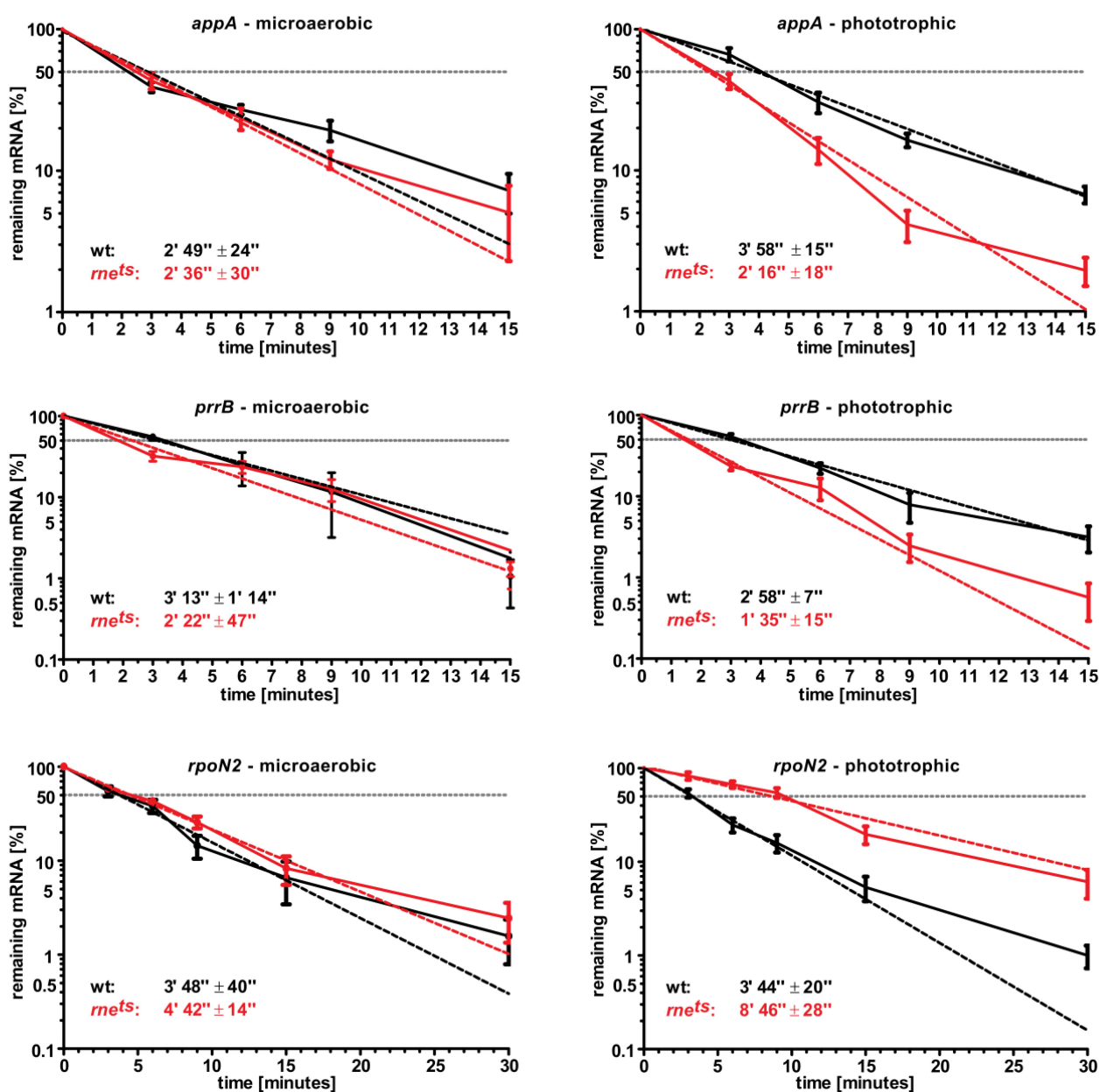
Figure 9. mRNA half-lives of *appA*, *prrB* and *rpoN2* under microaerobic and phototrophic growth conditions. The half-lives of mRNAs encoding important regulatory proteins for photosynthesis and motility were investigated under microaerobic and phototrophic conditions. Cultures were treated with 0.2 mg/ml rifampicin and samples were collected at the time points $t = 0$, 3, 6, 9, 15 and 30 minutes after addition of rifampicin. Total RNA was isolated using the hot phenol method, traces of DNA removed by DNase treatment and mRNA abundances relative to a spike-in RNA control of known sequence and quantity were determined by qRT-PCR using specific primers against *appA*, *prrB* or *rpoN2*. The decay of mRNA within biological triplicates of wild type (black) and *rne*^{ts} mutant (red) was fitted to semi-logarithmic trend lines (dashed lines). The standard deviation of the biological triplicates is shown as error bars. The calculated mRNA half-lives and their standard deviations are given in the bottom of each panel.

in the mutant. Our analysis revealed a strong enrichment of the TSS in the mutant exclusively under phototrophic conditions (Figure S10). In accordance with this observation the half-life of *rpoN2* is strongly increased in the mutant under phototrophic conditions (about 4 min 42 sec under microaerobic conditions, 8 min 46 sec in phototrophic conditions), while the half-life is the same under both growth conditions in the wild type (about 3 min 48 sec and 3 min 44 sec) (Figure 9). Higher RNA stability in the mutant can e.g. result

from impeded 5' end-dependent degradation pathway. The opposite effects of RNase E (destabilizing versus stabilizing) during phototrophic growth on *appA*, *prrB* versus *rpoN2* expression correlates well with the different expression patterns of cluster 3 and cluster 6 mRNAs. Despite the distinct expression pattern of cluster 3 RNAs, we did not observe a clear effect of RNase E on the swimming motility of *R. sphaeroides* under phototrophic conditions (data not shown).

Concluding remarks and outlook

Although an impact of ribonucleases on the bacterial transcriptome is described in several studies (e.g. [15,56–61]), such strong effects of an RNase on certain growth conditions as observed for *R. sphaeroides* ([21]; Figure 2 this study) are rare. In *E. coli* inactivation of the *rne* gene results in loss of colony forming ability on solid media [62] and in filamentous growth in liquid culture [63]. The filamentous phenotype was attributed to an effect of RNase E on the FtsZ/FtsA ratio [64]. Furthermore, a role of RNases in stress response is well established [15,65–69].

The present study links expression patterns of mRNAs under different growth conditions to the action of RNase E. A certain distribution of cleavage sites and enriched 5' ends in the mutant in defined mRNA clusters contributes to the observed expression pattern of those mRNA clusters. Furthermore, the action of RNase E on mRNAs for regulatory proteins indirectly affects their regulons. Indeed, the effect of RNase E on expression of photosynthesis genes and their regulators fits to the observed growth phenotype. An open question remains, why RNase E cleavages and enriched 5' ends in the mutant show such variation under the different growth conditions?

Our differential expression analysis hints to higher *rne* mRNA levels under aerobic conditions compared to phototrophic conditions in the wild type (Figure 3C) and in the mutant strain (data not shown). However, the quantification of mRNA levels gives no information on the RNase E activities under different conditions and if RNase E level/activity would vary between aerobic and phototrophic growth conditions, we should see a similar effect on all mRNAs that are recognized by RNase E, which is not the case. Nevertheless, we established a reporter assay to test for RNase E activity under different growth conditions. A short 89 nt sequence containing a well-defined RNase E recognition site was cloned in front of the mVenus reporter gene (Figure S2). This construct was transferred to the wild type and the *rne*[ts] cells by diparental conjugation and the resulting fluorescence was determined under the different growth conditions. The fluorescence caused by this construct was compared to the reporter construct without the newly incorporated RNase E cleavage site to include all putative effects of RNase E on other parts of the resulting mRNA. In the wild type strain the reporter with cleavage site showed much less activity than the control under all conditions (Figure 10). This difference was much smaller in the *rne*[ts] mutant. Figure 10 demonstrates that the biggest influence of RNase E on the activity of the reporter is seen under phototrophic conditions (about 6.8-fold difference between wild type and mutant; aerobic and microaerobic growth: about 3-fold difference). We cannot make confident conclusions about the total RNase activities under the different conditions, since the growth conditions also influence the activity of the reporter protein, but it is clear that phototrophic conditions differ from chemotrophic conditions in the ratio of RNase E activity in wild type and *rne*[ts] mutant. These strong differences in activity may well account for the strong effect of reduced RNase E activity especially during phototrophic growth but does not explain that not all RNAs with RNase E cleavage sites are affected.

It is also conceivable that the growth conditions affect RNA structure and subsequently substrate recognition by RNase E. Such changes may be influenced by the sequence and may thus be very different for individual RNAs. We also have to consider that not only ribonuclease and substrate are involved in the cleavage process. It was reported that the composition and activity of the degradosome complex in *R. capsulatus* vary under different oxygen concentrations [23]. Since the degradosome complexes in *E. coli* and *R. sphaeroides* vary, the oxygen condition may have different influence on the composition and activity of the degradosome in the *rne*[ts] mutant. Due to the binding of the *E. coli* enzyme to the cytoplasmic membrane, intracellular membranes may also have different effects on the activity of the degradosomes in the wild type and the *rne*[ts] strain. However, as not only phototrophic cells but also microaerobic cells are full of
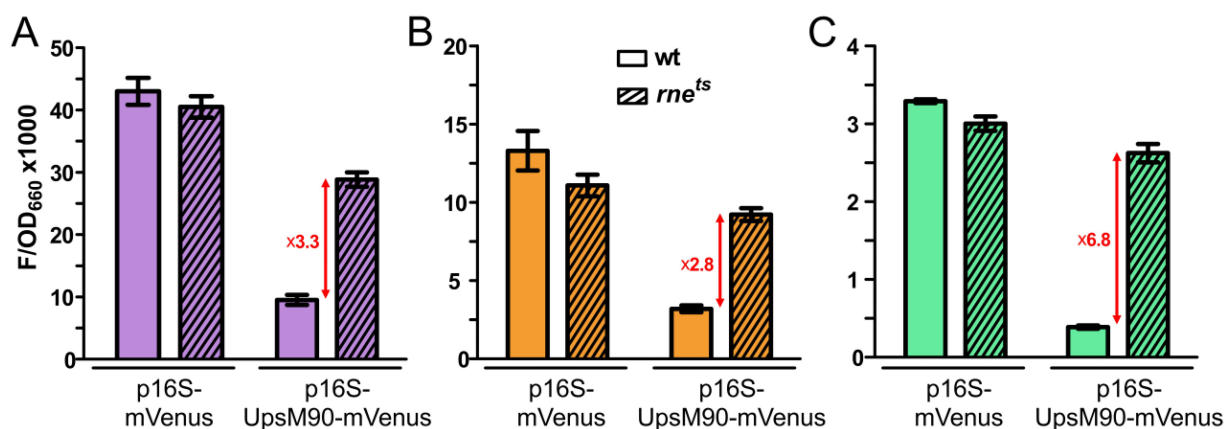

Figure 10. RNase E activity reporter measurements under aerobic, microaerobic and phototrophic growth conditions. The fluorescence intensity of mVenus was measured in biological triplicates *in vivo* under aerobic (A), microaerobic (B) and phototrophic (C) conditions, normalized by subtraction of the background fluorescence from an empty vector control and divided to the optical density OD_{660}. The standard deviations are given as error bars. Cells carrying the plasmid pPHU-p16s-mVenus represent a control, where the mVenus open reading frame is under transcriptional control of the constitutive 16S rRNA promoter from *R. sphaeroides*. pPHU-p16S-Upsm90-mVenus was used to assess RNase E activity by introduction of an 89 nt 5' UTR directly upstream of the mVenus open reading frame, harbouring a well characterized RNase E cleavage site originating from the small RNA UpsM of *R. sphaeroides*.

intracytoplasmic membrane vesicles, this is unlikely to account for the higher number of RNase E cleavage sites under phototrophic conditions.

It is also conceivable that the substitution of the native *R. sphaeroides rne* gene by a variant of the gammaproteobacterium *E. coli* contributes to the disruption of posttranscriptional gene expression regulation. As mentioned above, this could be due to the different architectures of the two enzymes (presence of the membrane targeting sequence and variances in protein interaction sites on the scaffold domain), but also to different activities of the catalytic RNase domains. Differentially specialized substrate recognition may be a possible factor that can lead to defective RNA processing. However, our analyses revealed that the vast majority of 5' end positions are identical in both strains. As the bacterial RNA degradosome is a very complex machinery, it is hard to distinguish between distinct effects of the single components (RNase E interaction partners or catalysis by RNase E itself) in our analysis.

Additionally, RNA chaperones like Hfq [70–72] or CsrA [73] play an important role in RNase E-mediated cleavage as well as adapter proteins like RapZ [74] or RNase E inhibitors like RraA in *E. coli* [75]. An *R. sphaeroides* strain lacking the Hfq protein has a pleiotropic phenotype including altered pigmentation and photooxidative stress resistance [76]. Recently, the DUF1127 protein CcaF1 was identified as a new type of RNA binding protein in *R. sphaeroides* and shown to assist in RNase E-dependent RNA processing [31]. CcaF1 has an important function in stress defence. *hfq* and *ccaF1* mRNA levels were similar under microaerobic and phototrophic conditions. We conclude that an effect of these RNA-binding proteins on RNase E mediated cleavage is unlikely to account for the observed growth-dependent effects of RNase E on the transcriptome, but cannot exclude post-transcriptional regulation of *hfq* or *ccaF1* expression. A second DUF1127 protein of *R. sphaeroides*, RSP_0557, was also shown to bind to many RNAs and to affect their levels [31]. Under phototrophic conditions RSP_0557 mRNA levels are much higher than under microaerobic and aerobic growth in the wild type. In the mutant, similar low RSP_0557 mRNA levels are observed under both conditions. Therefore, RSP_0557 may be a candidate for a mediator of growth-dependent RNA cleavage for a specific set of transcripts. Interestingly, the RSP_0557 mRNA (about 340 nt) possesses one of the highest *bona fide* RNase E cleavage site densities under phototrophic growth conditions (12 cleavage sites), and contains considerably less cleavage sites under microaerobic conditions (two cleavage sites) (Figure S11). An influence of RSP_0557 abundance on RNase E-dependent cleavage and of RNase E on RSP_0557 abundance would constitute a feed-back mechanism. Such regulatory loops put considerable constrains to the analysis of the role of individual components in a network. It is known, that RSP_0557 expression is controlled by the RpoHI/HII alternative sigma factors [77]. As a consequence, RSP_0557 mRNA increases during transition to stationary phase [42], in response to high oxygen levels, and under heat stress [78]. Thus, growth conditions influence RSP_0557 levels also independently of RNase E. The role of RSP_0557 as RNA chaperone requires, however, further analyses.

It is unlikely that the exact mechanisms behind the influence of growth conditions on RNase E-mediated cleavage can be identified by global studies. It will be necessary to select some RNase E substrates and to include different mutants for ribonucleases, transcriptional regulators and RNA-binding proteins. Unfortunately, it will not be possible to use defined *in vitro* systems for such studies. While the *in vitro* systems can limit the number of involved RNAs and proteins, they do not allow to look at the effect of environmental factors and growth conditions.

In summary, our data set provides insights into direct (RNase E-mediated RNA processing) and indirect (RNase E-dependent abundance of transcriptional regulators) effects that contribute to the strong impact of RNase E on growth under different environmental conditions. Especially the effect of RNase E on the stability of RNAs for important regulators of photosynthesis genes indirectly affects the expression of many photosynthesis genes and consequently the formation of photosynthetic complexes and phototrophic growth. The study underlines the importance of RNases in the adaptation of bacteria to changing growth conditions.

Data availability statement

The FASTQ files of all replicates from RNA sequencing are available in the NCBI Gene Expression Omnibus (GEO) repository [79] with the accession number GSE200990. https://ncbi.nlm.nih.gov/geo/query/acc.cgi?acc=GSE200990

Disclosure statement

No potential conflict of interest was reported by the authors.

ORCID

Janek Börner http://orcid.org/0000-0003-4824-9393
Tobias Friedrich http://orcid.org/0000-0003-4014-8678
Marek Bartkuhn http://orcid.org/0000-0001-6872-9082
Gabriele Klug http://orcid.org/0000-0002-3527-5093

References

[1] Hördt A, López MG, Meier-Kolthoff JP, et al. Analysis of 1,000+ type-strain genomes substantially improves taxonomic classification of alphaproteobacteria. Front Microbiol. 2020;11:468.

[2] Shimada H, Iba K, Takamiya K. Blue-light irradiation reduces the expression of *puf* and *puc* Operons of *Rhodobacter sphaeroides* under semi-aerobic conditions. Plant Cell Physiol. 1992;33:471–475.

[3] Braatsch S, Gomelsky M, Kuphal S, et al. A single flavoprotein, AppA, integrates both redox and light signals in *Rhodobacter sphaeroides*. Mol Microbiol. 2002;45:827–836.

[4] Anthony JR, Newman JD, Donohue TJ. Interactions between the *Rhodobacter sphaeroides* ECF sigma factor, sigma(e), and its anti-sigma factor, ChrR. J Mol Biol. 2004;341:345–360.

[5] Nuss AM, Glaeser J, Klug G. RpoH(II) activates oxidative-stress defense systems and is controlled by RpoE in the singlet oxygen-dependent response in *Rhodobacter sphaeroides*. J Bacteriol. 2009;191:220–230.

[6] Nuss AM, Glaeser J, Berghoff BA, et al. Overlapping alternative sigma factor regulons in the response to singlet oxygen in *Rhodobacter sphaeroides*. J Bacteriol. 2010;192:2613–2623.

[7] Dufour YS, Imam S, Koo BM, et al. Convergence of the transcriptional responses to heat shock and singlet oxygen stresses. PLoS Genet. 2012;8:e1002929.

[8] Bathke J, Konzer A, Remes B, et al. Comparative analyses of the variation of the transcriptome and proteome of *Rhodobacter sphaeroides* throughout growth. BMC Genomics. 2019;20:358.

[9] Klug G, Adams CW, Belasco J, et al. Biological consequences of segmental alterations in mRNA stability: effects of deletion of the intercistronic hairpin loop region of the *Rhodobacter capsulatus puf* operon. Embo J. 1987;6:3515–3520.

[10] Mank NN, Berghoff BA, Hermanns YN, et al. Regulation of bacterial photosynthesis genes by the small noncoding RNA PcrZ. Proc Natl Acad Sci U S A. 2012;109:16306–16311.

[11] Billenkamp F, Peng T, Berghoff BA, et al. A cluster of four homologous small RNAs modulates C1 metabolism and the pyruvate dehydrogenase complex in *Rhodobacter sphaeroides* under various stress conditions. J Bacteriol. 2015;197:1839–1852.

[12] Eisenhardt KMH, Reuscher CM, Klug G. PcrX, an sRNA derived from the 3'- UTR of the *Rhodobacter sphaeroides puf* operon modulates expression of *puf* genes encoding proteins of the bacterial photosynthetic apparatus. Mol Microbiol. 2018;110:325–334.

[13] Reuscher CM, Klug G. Antisense RNA asPcrL regulates expression of photosynthesis genes in *Rhodobacter sphaeroides* by promoting RNase III-dependent turn-over of *puf* mRNA. RNA Biol. 2021;18:1445–1457.

[14] Grützner J, Remes B, Eisenhardt KMH, et al. sRNA-mediated RNA processing regulates bacterial cell division. Nucleic Acids Res. 2021;49:7035–7052.

[15] Spanka DT, Reuscher CM, Klug G. Impact of PNPase on the transcriptome of *Rhodobacter sphaeroides* and its cooperation with RNase III and RNase E. BMC Genomics. 2021;22:106.

[16] Chen CYA, Beatty TJ, Cohen SN, et al. An intercistronic stem-loop structure functions as an mRNA decay terminator necessary but insufficient for *puf* mRNA stability. Cell. 1988;52:609–619.

[17] Klug G, Cohen SN. Combined actions of multiple hairpin loop structures and sites of rate-limiting endonucleolytic cleavage determine differential degradation rates of individual segments within polycistronic *puf* operon mRNA. J Bacteriol. 1990;172:5140–5146.

[18] Evguenieva-Hackenberg E, Klug G. Chapter 7 RNA degradation in archaea and gram-negative bacteria different from *Escherichia coli*. In: Condon C, editor. Progress in molecular biology and translational science. Amsterdam, Boston: Elsevier Academic Press; 2009. pp. 275–317.

[19] Chidgey JW, Jackson PJ, Dickman MJ, et al. PufQ regulates porphyrin flux at the haem/bacteriochlorophyll branchpoint of tetrapyrrole biosynthesis via interactions with ferrochelatase. Mol Microbiol. 2017;106:961–975.

[20] Klug G. A DNA sequence upstream of the *puf* operon of *Rhodobacter capsulatus* is involved in its oxygen-dependent regulation and functions as a protein binding site. Mol Gen Genet. 1991;226:167–176.

[21] Förstner KU, Reuscher CM, Haberzettl K, et al. RNase E cleavage shapes the transcriptome of *Rhodobacter sphaeroides* and strongly impacts phototrophic growth. Life Sci Alliance. 2018;1: e201800080.

[22] Carpousis AJ, Campo N, Hadjeras L, et al. Compartmentalization of RNA degradosomes in bacteria controls accessibility to substrates and ensures concerted degradation of mRNA to nucleotides. Annu Rev Microbiol. 2022;76:533–552.

[23] Jäger S, Hebermehl M, Schiltz E, et al. Composition and activity of the *Rhodobacter capsulatus* degradosome vary under different oxygen concentrations. J Mol Microbiol Biotechnol. 2004;7:148–154.

[24] Golecki JR, Oelze J. Differences in the architecture of cytoplasmic and intracytoplasmic membranes of three chemotrophically and phototrophically grown species of the Rhodospirillaceae. J Bacteriol. 1980;144:781–788.

[25] Aït-Bara S, Carpousis AJ. RNA degradosomes in bacteria and chloroplasts: classification, distribution and evolution of RNase E homologs. Mol Microbiol. 2015;97:1021–1135.

[26] van Niel CB. The culture, general physiology, morphology, and classification of the non-sulfur purple and brown bacteria. Bacteriol Rev. 1944;8:1–118.

[27] Weber L, Thoelken C, Volk M, et al. The conserved Dcw gene cluster of *R. sphaeroides* is preceded by an uncommonly extended 5' leader featuring the sRNA UpsM. PLoS ONE. 2016;11: e0165694.

[28] Remes B, Berghoff BA, Förstner KU, et al. Role of oxygen and the OxyR protein in the response to iron limitation in *Rhodobacter sphaeroides*. BMC Genomics. 2014;15:794.

[29] Janzon L, Löfdahl S, Arvidson S. Evidence for a coordinate transcriptional control of alpha-toxin and protein a synthesis in *Staphylococcus aureus*. FEMS Microbiol Lett. 1986;33:193–198.

[30] Damm K, Bach S, Müller KMH, et al. Impact of RNA isolation protocols on RNA detection by Northern blotting. Methods Mol Biol. 2015;1296:29–38.

[31] Grützner J, Billenkamp F, Spanka D-T, et al. The small DUF1127 protein CcaF1 from *Rhodobacter sphaeroides* is an RNA-binding protein involved in sRNA maturation and RNA turnover. Nucleic Acids Res. 2021;49:3003–3019.

[32] Pfaffl MW. A new mathematical model for relative quantification in real-time RT-PCR. Nucleic Acids Res. 2001;29:e45.

[33] Förstner KU, Vogel J, Sharma CM. Reademption - a tool for the computational analysis of deep-sequencing-based transcriptome data. Bioinformatics. 2014;30:3421–3423.

[34] R Core Team. A language and environment for statistical computing. Vienna, Austria: R foundation of statistical computing; 2021.

[35] Backman TWH, Girke T. systemPipeR: NGS workflow and report generation environment. BMC Bioinf. 2016;17:388.

[36] Love MI, Huber W, Anders S. Moderated estimation of fold change and dispersion for RNA-seq data with DESeq2. Genome Biol. 2014;15:550.

[37] Remes B, Rische-Grahl T, Müller KMH, et al. An RpoHI-dependent response promotes outgrowth after extended stationary phase in the Alphaproteobacterium *Rhodobacter sphaeroides*. J Bacteriol. 2017;199.

[38] Quinlan AR, Hall IM. Bedtools: a flexible suite of utilities for comparing genomic features. Bioinformatics. 2010;26:841–842.

[39] Korotkevich G, Sukhov V, Budin N, et al. Fast gene set enrichment analysis. bioRxiv. 2016 [2021 Feb 1]. pre-print: not peer-reviewed. DOI:10.1101/060012

[40] Benjamini Y, Hochberg Y. Controlling the false discovery rate: a practical and powerful approach to multiple testing. J R Stat Soc Ser B Methodol. 1995;57:289–300.

[41] Liao Y, Smyth GK, Shi W. The R package Rsubread is easier, faster, cheaper and better for alignment and quantification of RNA sequencing reads. Nucleic Acids Res. 2019;47:e47.

[42] McIntosh M, Eisenhardt K, Remes B, et al. Adaptation of the Alphaproteobacterium *Rhodobacter sphaeroides* to stationary phase. Environ Microbiol. 2019;21:4425–4445.

[43] Simon R, Priefer U, Pühler A. A broad host range mobilization system for *in vivo* genetic engineering: transposon mutagenesis in gram negative bacteria. Biotechnology. 1983;1:784–791.

[44] Pappas CT, Sram J, Moskvin OV, et al. Construction and validation of the *Rhodobacter sphaeroides* 2.4.1 DNA microarray: transcriptome flexibility at diverse growth modes. J Bacteriol. 2004;186:4748–4758.

[45] Klug G. Beyond catalysis: vitamin B12 as a cofactor in gene regulation. Mol Microbiol. 2014;91:635–640.

[46] Karls RK, Brooks J, Rossmeissl P, et al. Metabolic roles of a *Rhodobacter sphaeroides* member of the sigma32 family. J Bacteriol. 1998;180:10–19.

[47] Peng T, Berghoff BA, Oh JI, et al. Regulation of a polyamine transporter by the conserved 3' UTR-derived sRNA SorX confers resistance to singlet oxygen and organic hydroperoxides in *Rhodobacter sphaeroides*. RNA Biol. 2016;13:988–999.

[48] Srivastava AK, Schlessinger D. Mechanism and regulation of bacterial ribosomal RNA processing. Annu Rev Microbiol. 1990;44:105–129.

[49] Evgueneva-Hackenberg E. Bacterial ribosomal RNA in pieces. Mol Microbiol. 2005;57:318–325.

[50] Deutscher MP. Chapter 9 Maturation and degradation of ribosomal RNA in bacteria. In: Condon C, editor. Progress in molecular biology and translational science. Amsterdam, Boston: Elsevier Academic Press; 2009. pp. 369–391.

[51] Rische T, Klug G. The ordered processing of intervening sequences in 23S rRNA of *Rhodobacter sphaeroides* requires RNase J. RNA Biol. 2012;9:343–350.

[52] Roh JH, Smith WE, Kaplan S. Effects of oxygen and light intensity on transcriptome expression in *Rhodobacter sphaeroides* 2.4.1. Redox active gene expression profile. J Biol Chem. 2004;279:9146–9155.

[53] Poggio S, Osorio A, Dreyfus G, et al. The four different sigma(54) factors of *Rhodobacter sphaeroides* are not functionally interchangeable. Mol Microbiol. 2002;46:75–85.

[54] Poggio S, Osorio A, Dreyfus G, et al. Transcriptional specificity of RpoN1 and RpoN2 involves differential recognition of the promoter sequences and specific interaction with the cognate activator proteins. J Biol Chem. 2006;281:27205–27215.

[55] Vega-Baray B, Domenzain C, Rivera A, et al. The flagellar set Fla2 in *Rhodobacter sphaeroides* is controlled by the CckA pathway and is repressed by organic acids and the expression of Fla1. J Bacteriol. 2015;197:833–847.

[56] Le Rhun A, Lécrivain AL, Reimegård J, et al. Identification of endoribonuclease specific cleavage positions reveals novel targets of RNase III in *Streptococcus pyogenes*. Nucleic Acids Res. 2017;45:2329–2340.

[57] Altuvia Y, Bar A, Reiss N, et al. *In vivo* cleavage rules and target repertoire of RNase III in *Escherichia coli*. Nucleic Acids Res. 2018;46:10380–10394.

[58] Broglia L, Lécrivain A-L, Renault TT, et al. An RNA-seq based comparative approach reveals the transcriptome-wide interplay between 3'-to-5' exoRnases and RNase Y. Nat Commun. 2020;11:1587.

[59] Duggal Y, Fontaine BM, Dailey DM, et al. RNase I modulates *Escherichia coli* motility, metabolism, and resistance. ACS Chem Biol. 2020;15:1996–2004.

[60] Hoffmann UA, Heyl F, Rogh SN, et al. Transcriptome-wide *in vivo* mapping of cleavage sites for the compact cyanobacterial ribonuclease E reveals insights into its function and substrate recognition. Nucleic Acids Res. 2021;49:13075–13091.

[61] Ifill G, Blimkie T, Lee AHY, et al. RNase III and RNase E influence posttranscriptional regulatory networks involved in virulence factor production, metabolism, and regulatory RNA processing in *Bordetella pertussis*. mSphere. 2021;6:e0065021.

[62] Deana A, Belasco JG. The function of RNase G in *Escherichia coli* is constrained by its amino and carboxyl termini. Mol Microbiol. 2004;51:1205–1217.

[63] Goldblum K, Apririon D. Inactivation of the ribonucleic acid-processing enzyme ribonuclease E blocks cell division. J Bacteriol. 1981;146:128–132.

[64] Tamura M, Lee K, Miller CA, et al. RNase E maintenance of proper FtsZ/FtsA ratio required for nonfilamentous growth of *Escherichia coli* cells but not for colony-forming ability. J Bacteriol. 2006;188:5145–5152.

[65] Goverde RL, Huis In't Veld JH, Kusters JG, et al. The psychrotrophic bacterium *Yersinia enterocolitica* requires expression of *pnp*, the gene for polynucleotide phosphorylase, for growth at low temperature (5 degrees C). Mol Microbiol. 1998;28:555–569.

[66] Apura P, Lorenzo VD, Arraiano CM, et al. Ribonucleases control distinct traits of *Pseudomonas putida* lifestyle. Environ Microbiol. 2021;23:174–189.

[67] Manasherob R, Miller C, Kim K, et al. Ribonuclease E modulation of the bacterial SOS response. PLoS ONE. 2012;7:e38426.

[68] Rosenzweig JA, Chopra AK. The exoribonuclease Polynucleotide Phosphorylase influences the virulence and stress responses of yersiniae and many other pathogens. Front Cell Infect Microbiol. 2013;3:81.

[69] Lejars M, Hajnsdorf E. RNase III participates in the adaptation to temperature shock and oxidative stress in *Escherichia coli*. Microorganisms. 2022;10:699.

[70] Vogel J, Luisi BF. Hfq and its constellation of RNA. Nat Rev Microbiol. 2011;9:578–589.

[71] Sauer E. Structure and RNA-binding properties of the bacterial LSm protein Hfq. RNA Biol. 2013;10:610–618.

[72] Wagner EGH. Cycling of RNAs on Hfq. RNA Biol. 2013;10:619–626.

[73] Stenum TS, Holmqvist E. CsrA enters Hfq's territory: regulation of a base-pairing small RNA. Mol Microbiol. 2022;117:4–9.

[74] Göpel Y, Papenfort K, Reichenbach B, et al. Targeted decay of a regulatory small RNA by an adaptor protein for RNase E and counteraction by an anti-adaptor RNA. Genes Dev. 2013;27:552–564.

[75] Lee K, Zhan X, Gao J, et al. RraA: a protein inhibitor of RNase E activity that globally modulates RNA abundance in *E. coli*. Cell. 2003;114:623–634.

[76] Berghoff BA, Glaeser J, Sharma CM, et al. Contribution of Hfq to photooxidative stress resistance and global regulation in *Rhodobacter sphaeroides*. Mol Microbiol. 2011;80:1479–1495.

[77] Müller KMH, Berghoff BA, Eisenhardt BD, et al. Characteristics of Pos19 - a small coding RNA in the oxidative stress response of *Rhodobacter sphaeroides*. PLoS ONE. 2016;11:e0163425.

[78] McIntosh M, Köchling T, Latz A, et al. A major checkpoint for protein expression in *Rhodobacter sphaeroides* during heat stress response occurs at the level of translation. Environ Microbiol. 2021;23:6483–6502.

[79] Edgar R, Domrachev M, Lash AE. Gene Expression Omnibus: NCBI gene expression and hybridization array data repository. Nucleic Acids Res. 2002;30:207–210.